Journal of Al-Azhar University Engineering Sector

Vol .20, No. 74, Junuary 2025, 155 - 171

FLEXURAL BEHAVIOR OF CONCRETE MEMBERS REINFORCED WITH BASALT FRP-STEEL WIRES COMPOSITE BARS: NUMERICAL AND EXPERIMENTAL STUDY

Yasser M. Mohammad[1*], Abd El-Kader A. Haridy[1], Abo El-Wafa M. El-Thakeb[2]

[1] Department of Civil Engineering, Faculty of Engineering, Al-Azhar University, Qena, Egypt.

[2] Department of Civil Engineering, Faculty of Engineering, Al-Azhar University, Naser City, Cairo, Egypt.

*Correspondence: Yasser_mahmoud@azhar.edu.eg

Citation:
Y. M. Mohmmad, A. A. Haridy and A. M. El-Thakeb, "Flexural Behavior of Concrete Members Reinforced with Basalt FRP-Steel Wires Composite Bars: Numerical and Experimental Study ", Journal of Al-Azhar University Engineering Sector, vol. 20, pp. 155 - 171, 2025.

Received: 02 November 2024

Revised: 10 December 2024

Accepted: 31 December 2024

Doi: 10.21608/auej.2025.335998.1732

ABSTRACT

Basalt FRP-steel composite bars address limitations of conventional steel and BFRP bars in harsh environments. This study evaluates flexural behavior through experimental and numerical methods, utilizing 3D nonlinear finite element analysis (ANSYS 15). Four concrete beams with varying reinforcement types were tested for load capacity, deflection, and cracking patterns. Results showed significant reductions in deflection and crack widths with hybrid reinforcement, improving flexural capacity. Theoretical predictions aligned with experimental and numerical outcomes, validating the proposed approach.

KEYWORDS: Experimental study, Flexural performance, BFRP bar, steel wire-basalt FRP composite bars, 3D nonlinear finite element analysis (NLFEA), theoretical analysis.

سلوك الانحناء للعناصر الخرسانية المسلحة بأسياخ مركبة من ألياف بوليمرات البازلت وأسلاك الحديد: دراسة عددية وتجريبية

ياسر محمود محمد[1*]، عبد القادر أحمد هريدي[1]، أبو الوفا محمد الثاقب عمر [2]

[1] قسم الهندسة المدنية، كلية الهندسة، جامعة الأزهر، قنا، مصر

[2] قسم الهندسة المدنية، كلية الهندسة، جامعة الأزهر، مدينة نصر، القاهرة، مصر

البريد الاليكتروني للباحث الرئيسي*: Yasser_mahmoud@azhar.edu.eg

الملخص

تعالج الأسياخ المركبة من ألياف البازلت والحديد كمادة ذات ممطوليه لمعالجة معامل المرونة المنخفض والسلوك القصيف لأسياخ ألياف البازلت وكذلك التغلب على الصدأ الذي يطرأ على أسياخ حديد التسليح وخصوصاً المعرضة منها لظروف بيئية قاسية. تقيم هذه الدراسة سلوك الانحناء للكمرات الخرسانية المسلحة بأسياخ ألياف البازلت أو الأسياخ المركبة من ألياف البازلت وأسلاك الحديد من خلال الأساليب التجريبية والعددية، باستخدام تحليل العناصر المحدودة غير الخطية ثلاثية الأبعاد (ANSYS 15). تم اختبار أربع كمرات خرسانية بسيطة الارتكاز معملياً تحت تأثير حمل إستاتيكي لدراسة كلا من مقاومة الانحناء والترخيم في

منتصف البحر وأنماط الشروخ وأسلوب الانهيار. أظهرت النتائج انخفاضًا كبيرًا في الترخيم وعرض الشقوق مع التسليح الهجين، مما أدى إلى تحسين قدرة الانحناء. تتوافق التوقعات النظرية مع النتائج التجريبية والعددية، مما يثبت صحة النهج المقترح.

الكلمات المفتاحية: الاختبار المعملي ،أداء الانحناء ، أسياخ ألياف البازلت ، الأسياخ المركبة من ألياف البازلت وأسلاك الحديد ، نمذجة العناصر المحدودة ، دراسة نظرية.

1. Introduction

One of the main factors affecting the service life of concrete structures reinforced with traditional steel bars is their rapid deterioration, particularly those susceptible to aggressive environments. The corrosion leads to reduced structural integrity and results in expensive maintenance and rehabilitation efforts to mitigate the corrosion issues [1]. Recently, fiber-reinforcing polymer FRP bars were employed in the concrete structures as the main reinforcement due to their superior tensile strength and remarkable corrosion resistance [2]. However, the brittle manner and low modulus of elasticity for FRP bars usually lead to large deflection and wide cracks. As a result, the serviceability limit state is commonly used as the governing criterion for designing FRP bar-reinforced concrete members [3]. Recently, several studies tried to address the shortcomings of both steel and FRP by integrating two different types of materials to enhance the properties of basalt fiber-reinforcing polymer FRP bars [4-10].

The flexural behavior of twelve concrete beams reinforced with different ratios of locally manufactured hybrid GFRP-steel wires bars were tested. The results demonstrated that increasing the hybrid reinforcement ratio resulted in a substantial increase in load capacity, ductility, and stiffness [11]. Furthermore, six concrete beams were reinforced with either steel, GFRP, or hybrid GFRP-steel wires with different GFRP-to-steel wires ratios were examined. The test results revealed that the significant increase of 40 to 50% in load capacity for beams reinforced with hybrid GFRP-steel wire bars were observed [12]. Furthermore, Mohamed Abo Elyazed et al. tested five simply supported slabs reinforced with glass-steel wires, utilizing steel/GFRP ratios of 6.25%, 12.5%, and 22%. The results compared with slabs reinforced with either conventional steel or GFRP bars [13]. Test results indicated a slight reduction in the ultimate load capacity and a significant enhancement in the ductility of slabs reinforced with hybrid FRP bars in comparison to those reinforced with GFRP. The current study conducted an experimental evaluation to assess the flexural performance of concrete beams reinforced with various types of locally manufactured basalt fiber-steel wires composite bars presented in [14]. Then, compare results with concrete beams reinforced with either basalt FRP or conventional steel bars. 3D nonlinear finite element analysis (ANSYS 15) was conducted to calibrate and verify the behavior of the tested concrete beams. Moreover, expand the nonlinear finite element model to include another two concrete beams reinforced with different types of basalt fibers-steel wires composite bars. Theoretical analysis in accordance with ACI440.1R-15 [15] was developed to predict the ultimate load of the tested beam. The theoretical results were compared with both experimental and FEA results. This paper aims to evaluate the flexural and serviceability performance of concrete beams reinforced with either basalt FRP bars or basalt fiber-steel wires composite bars by means of numerical and theoretical approaches.

2. Experimental Program

2.1 Material

2.1.1 Concrete

The concrete mix used in this investigation was intended to have a compressive strength of about 36 MPa after 28 days. Three standard cylinders with dimensions of 150 × 300 mm were subjected to uniaxial compressive load on the test date for each beam. The average concrete compressive strength ($f_c^{`}$) was 37.8 MPa for beams (B1 and B2) and 36.45 MPa for beams (B3 and B4). **Table. 1** lists the concrete mix proportions by weight.

Table. 1 Mixing proportions of concrete materials (KN/m^3)

Cement ($kN/m^{3)}$	Fine aggregate ($kN/m^{3)}$	Coarse aggregate ($kN/m^{3)}$	Water ($Liter/m^{3)}$	Superplasticizer ($Liter/m^{3)}$
4.50	7.30	11.70	155	9.8

2.1.2 Reinforcement

The mechanical properties for steel bars, locally manufactured basalt FRP bars, and basalt fiber-steel wires composite bars were used as the main reinforcement for the tested beams, and FEA models were depending on the test results that were reported in [14]. **Table. 2** detailed the properties of all reinforcement bars, whereas **Fig. 1** illustrated the curve of the stress-strain relationship for both basalt FRP bars and basalt fiber-steel wires composite bars.

Table. 2 Mechanical properties of steel bar, basalt-FRP bar and basalt fiber- steel wires composite bars [14]:

Specimen	Reinforcement Type	Nominal Diameter (mm)	Inner Core Diameter (mm)	Steel wires-to-BFRP ratio (%)	Modulus of Elasticity (GPa)	Yield Strength (MPa)	Maximum Strength (MPa) f_{sfu}	Maximum Strain (%) ε_{sfu}
Steel bar	S10	9.8	------	------	195.00	522.43	692.22	17.93
A	B-SW-0	10	------	0	47.94	------	1242.16	2.63
C	B-SW-12%	10	3 Ø 2	12%	51.16	------	1184.68	2.41
D	B-SW-20%	10	5 Ø 2	20%	55.74	------	1154.66	2.16
E	B-SW-28%	10	7 Ø 2	28%	62.90	------	1230.15	2.04
F	B-SW-36%	10	9 Ø 2	36%	77.89	------	1300.50	1.77

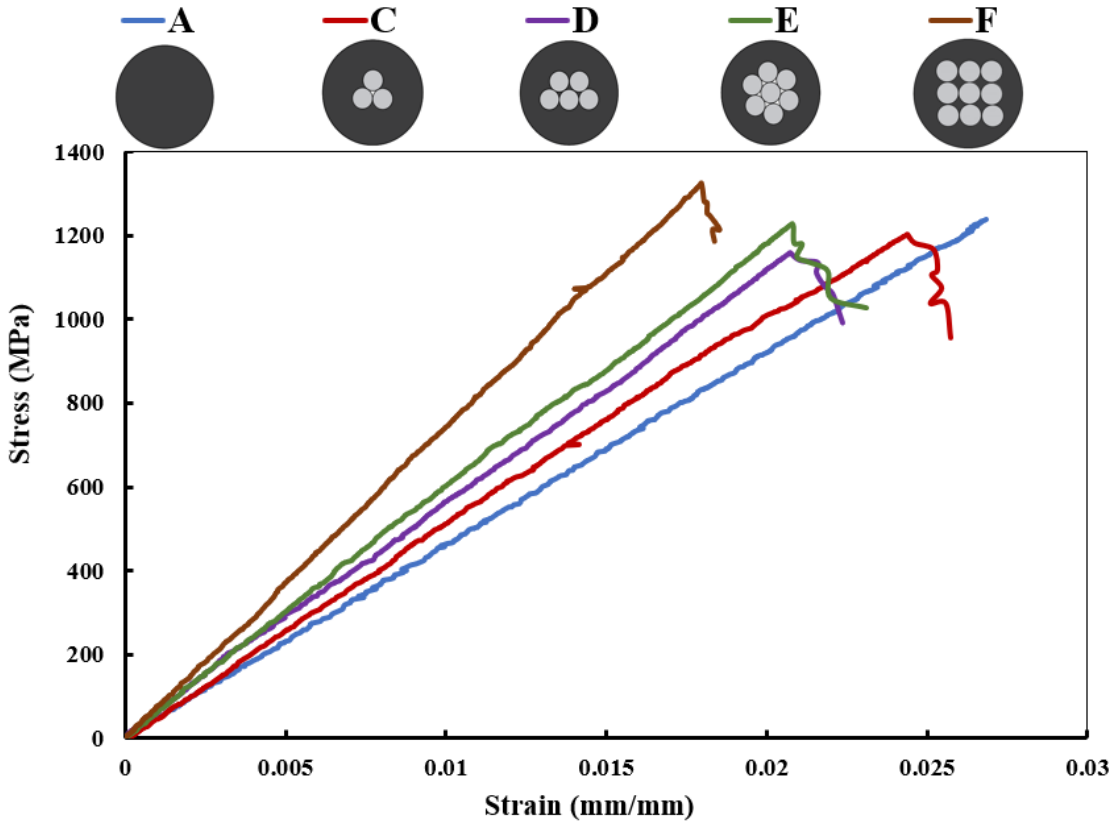

Fig.1. Stress-Strain Curves for basalt FRP and basalt fiber-steel wires composite bars.

2.2 Specimen Design

Four simply supported reinforced concrete beams, with an overall length of 2250 mm and a cross-sectional dimension of 150 mm in width and 300 mm in height. All beams were tested under four-point static load. The main parameter considered in this study was the type of main reinforcement. Beams B1 and B2 served as control beams and were reinforced with three traditional steel bars or locally produced basalt FRP bars, respectively, with a nominal diameter of 10 mm. Furthermore, beams B3 and B4 were reinforced with three bars of type B-SW-20% and B-SW-36%, respectively. All beams incorporated two 8 mm-diameter steel bars as compression reinforcement and 8 mm-diameter steel stirrups spaced at 100 mm to prevent shear failure. All beams were designed with a 30 mm concrete cover and 270 mm effective depth, as shown in **Fig. 2**. The FRP beams were intended to be over-reinforced concrete sections, such that the FRP reinforcement ratio (ρ_f) exceeded 1.4 times the balanced ratio of the FRP reinforcement (ρ_{fb}) according to ACI440.1R-15 [15]. Table. 3 summarized the tested beams details.

Table. 3 Tested concrete beams details.

Beam No.	RFT Type	D (mm)	($\hat{f_c}$) MPa	A_s (mm^2)	ρ_s %	ρ_f %	ρ_{fb} %	ρ_f / ρ_{fb}	Section Type
B1	S10	9.80	37.80	226.29	0.55	----	----	----	U - S
B2	B-SW-0	10.00	37.80	235.59	----	0.581	0.208	2.78	O - S
B3	B-SW-20%	10.00	36.45	235.59	----	0.581	0.268	2.16	O - S
B4	B-SW-36%	10.00	36.45	235.59	----	0.581	0.286	2.02	O - S
*B5	B-SW-12%	10.00	36.45	235.59	----	0.581	0.237	2.45	O - S
*B6	B-SW-28%	10.00	36.45	235.59	----	0.581	0.264	2.19	O - S

*B =basalt, SW = steel wires, D = reinforcement diameter (mm), ($\hat{f_c}$) = Concrete Compressive Strength (MPa), As = bottom reinforcement area (mm2), ρ_s = ratio of steel reinforcement, ρ_{fb} = ratio of balanced FRP reinforcement, ρ_f = ratio of FRP reinforcement, U – S = under reinforced concrete section, O – S = over reinforced concrete section.
*B5 and *B6 only finite element analysis

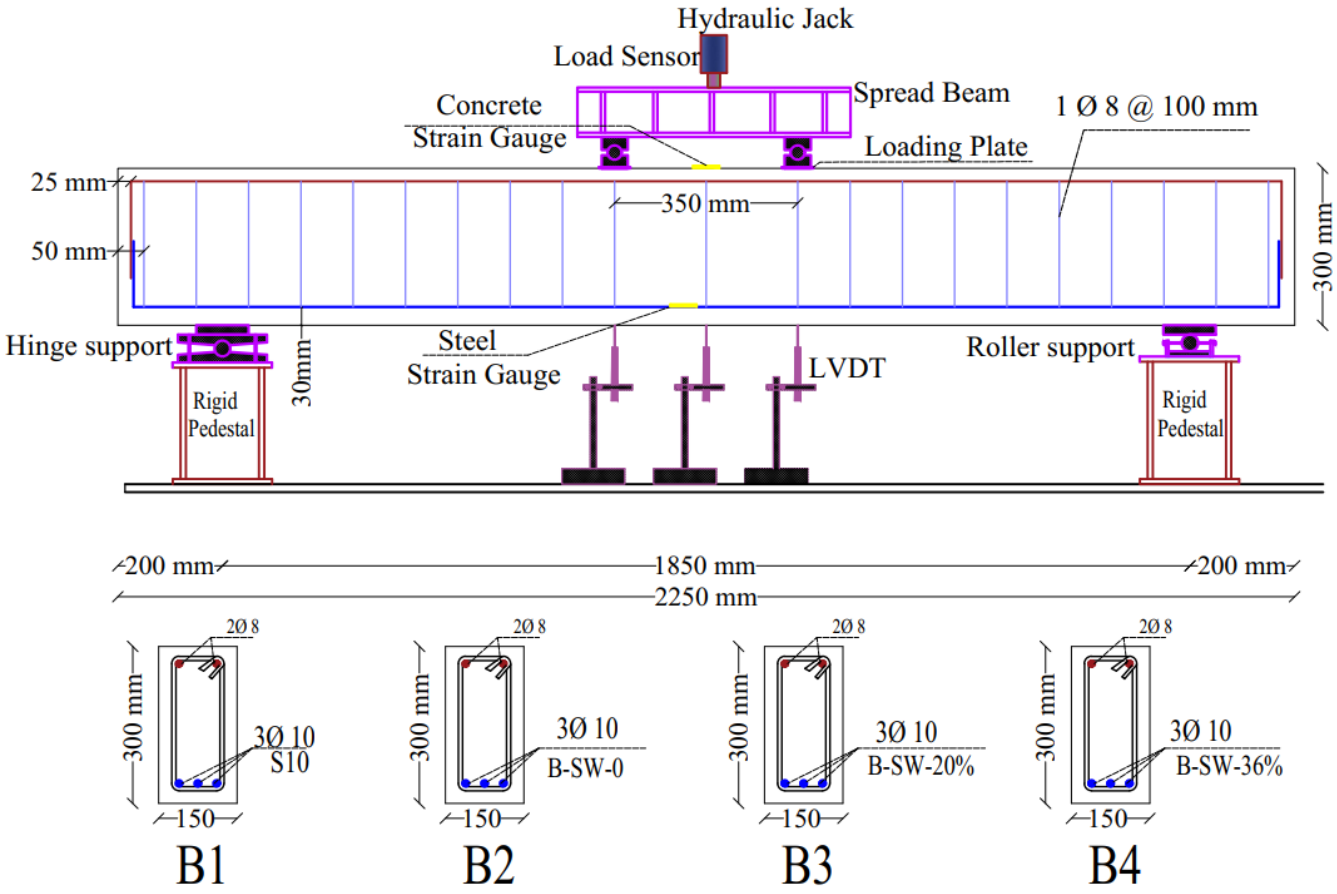

Fig. 2. Schematic view for test setup and beams the cross-sections.

2.3 Test Setup and Instruments

In this investigation, a four-point flexural test was conducted over a clear span of 1850 mm and a shear span of 350 mm as detailed in **Fig. 2**. To facilitate cracks observation, all beams were white-painted and marked with a 100 mm grid. During testing, strain variation in the main tensile reinforcement was monitored using 5 mm strain gauges affixed at the mid-span location on the tension bars. Furthermore, compressive strains in the concrete were assessed using a 60 mm strain gauge bonded to the upper surface of the concrete in the compression zone. Three Linear Variable Differential Transformers (LVDTs) were affixed to three bottom positions (loading and midspan points). The (LVDTs) were connected to a data acquisition system for continuous data recording. As shown in **Fig 3**, beams underwent testing using a 400 kN capacity testing machine. Where the load was applied in a rate of 0.2 kN with a hydraulic jack and a load cell for accurate monitoring and recording of the applied load. All cracks were documented during the loading processes until failure occurred.

Fig. 3. Experimental test setup and steel arrangement of beams B1, B2, B3, and B4.

3. Nonlinear Finite Element Analysis

3.1 General

Three-dimensional numerical models were developed using ANSYS 15 [16] to evaluate the flexural performance of the tested beams B1, B2, B3, and B4. Subsequent to the verification of the numerical models, a parametric study was performed to assess the flexural behavior of concrete beams B5 and B6, which were reinforced with three basalt fiber-steel wires composite bars of types B-SW-12% and B-SW-28%, respectively.

3.2 Finite elements types and materials

Four elements were selected and used from the ANSYS's elements library to simulate the flexural properties of concrete beams reinforced with steel or FRP bars as shown in **Fig 4.**

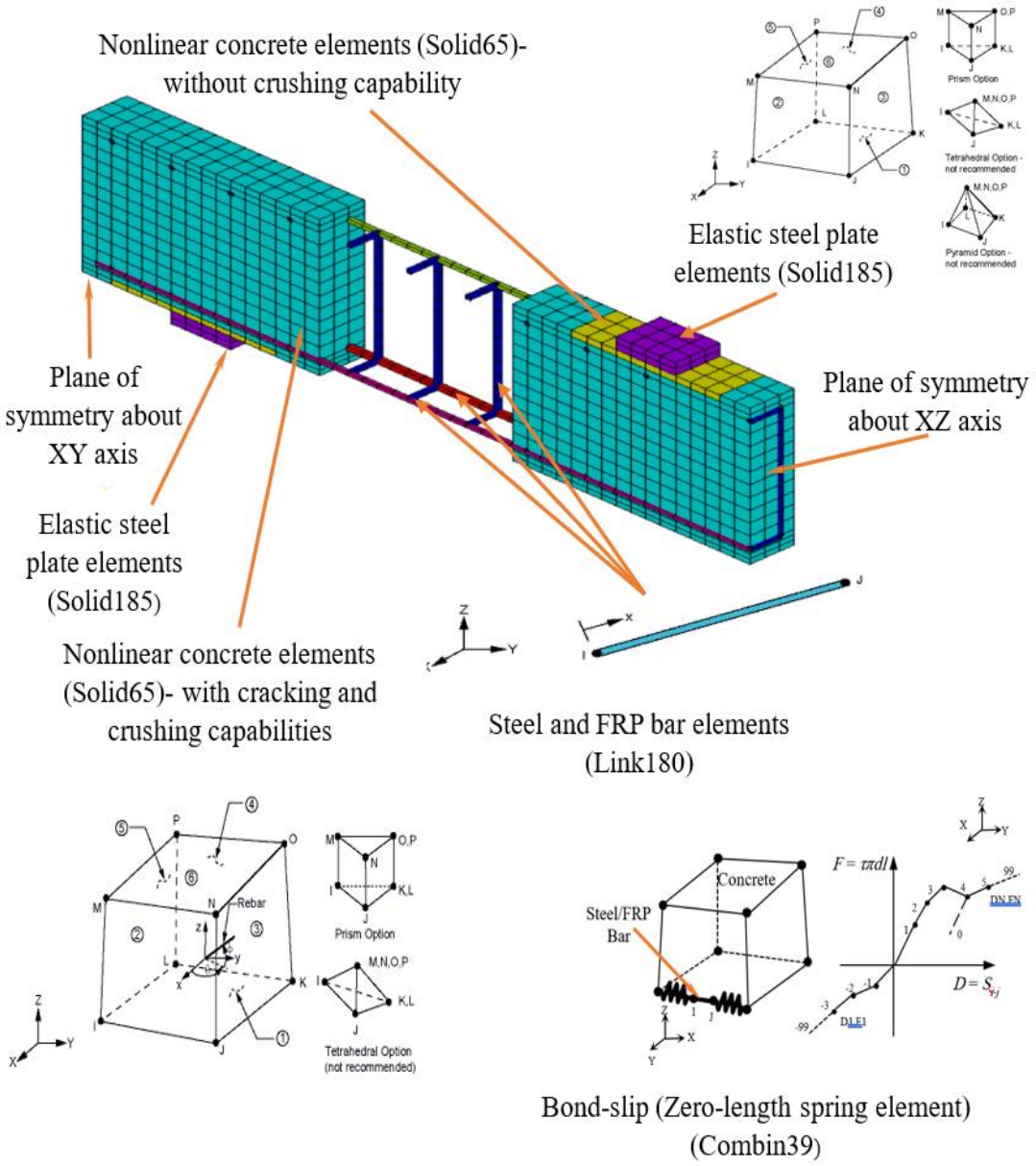

Fig. 4. Finite elements types.

3.2.1 Concrete

The concrete behavior within the ANSYS 15 [16] numerical models was simulated using the three-dimensional eight-nodes solid element SOLID 65. This element, possessing three translational degrees of freedom at each node, allows for modeling of plastic deformation, as well as cracking and crushing in three orthogonal directions. Before cracking or crushing, concrete is supposed to be an isotropic elastic material. After cracking, the concrete is assumed to be orthotropic and stiff. Crushing causes significant loss in concrete rigidity in all directions. To avoid premature concrete cover crushing and numerical convergence problems for elements adjacent to loading and support plates, the crushing capability was ignored, and the concrete compressive strength was established as displayed in **Fig.4**. To ensure accurate modeling for concrete properties, the linear and nonlinear isotropic hardening is considered. For linear behavior, the initial Young's modulus was defined according to ACI 318–19 [17]. Also, the Poisson's ratio value was determined to be 0.2. For non-linear behavior, the Hognestad model [18] was used to define the multilinear isotropic hardening

behavior as plotted in **Fig. 5a**. In addition, the concrete tensile stress-strain response was evaluated according to ACI 318–19 [17] as displayed in **Fig. 5b**. For modeling non-metal placidity, open and closed shear transfer coefficients were considered.

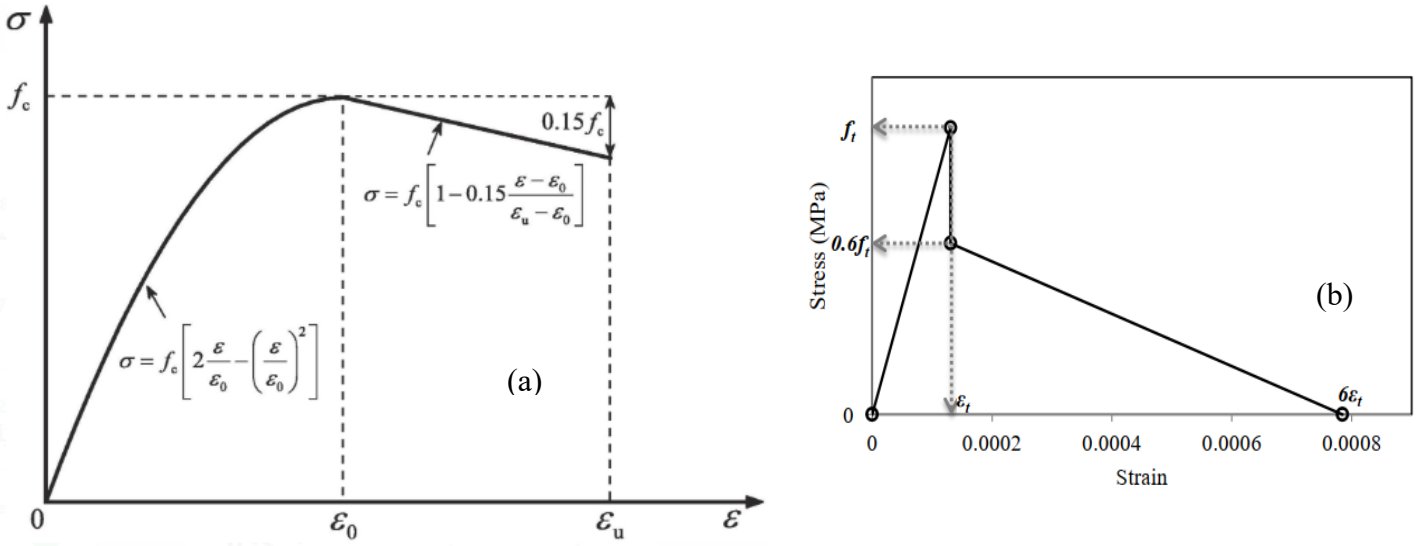

Fig. 5 (a) concrete compressive according to Hognestad model [18], and (b) concrete tensile stress-strain response according to ACI 318–19[17].

3.2.2 Steel and FRP bars

The 3-D spar structural bar element LINK180 was employed to represent longitudinal steel bars, steel stirrups, and fiber-reinforced polymer (FRP) bars. LINK180 is a two-nodes straight element that exposes plastic deformation; each node possesses three degrees of freedom, allowing for translations through the x, y, and z axes. Linear and bilinear isotropic hardening behaviors are needed to accurately model the longitudinal steel reinforcement and stirrups. Both the modulus of elasticity (EX) and Poisson's ratio (PRXY) were adopted in linear behavior. Furthermore, bilinear isotropic is addressed to the present stress-strain curve for steel bars and stirrups incorporating a strain hardening ratio of 0.01. Furthermore, linear elastic behavior was enough to present FRP bar behavior with Poisson's ratio (PRXY) of 0.2. **Fig. 6** illustrated the bilinear and linear elastic stress-strain model for the steel and FRP bars, respectively.

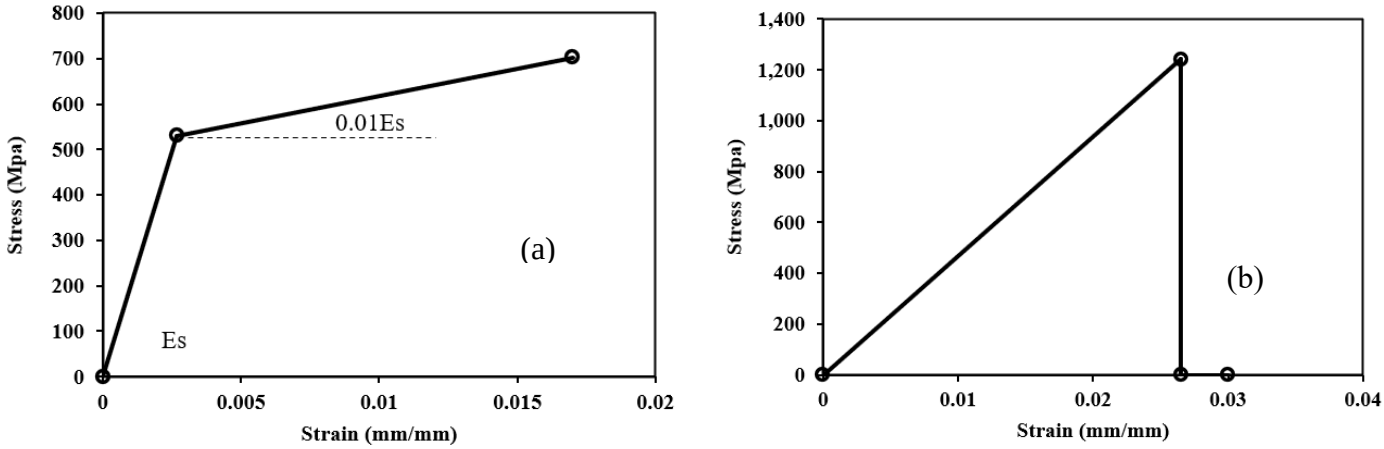

Fig. 6 (a) bilinear stress-strain curve for steel bars, and (b) FRP bars linear-elastic model.

3.2.3 Loading and supporting steel plates

The SOLID185 element is utilized to model the loading and support steel plates. SOLID185 is a solid element defined by eight nodes; each node possesses three degrees of freedom, allowing for translations through the x, y, and z axes. The stress-strain behavior is considered to be linear with Poisson's ratio (PRXY) of 0.3.

3.2.4 Concrete-reinforcement interfaces

COMBIN39 is a dimensionless unidirectional spring element with longitudinal uniaxial tension-compression. According to bond-slip modeling, the interface between the concrete and reinforcement is represented using three degrees of freedom. This element models the slippage between tension reinforcement and concrete in the longitudinal direction (x-axis) by applying a non-linear force-displacement relationship. The element uses node coupling to prevent movement in the perpendicular directions (y and z), as illustrated in **Fig. 7** [19], [20].

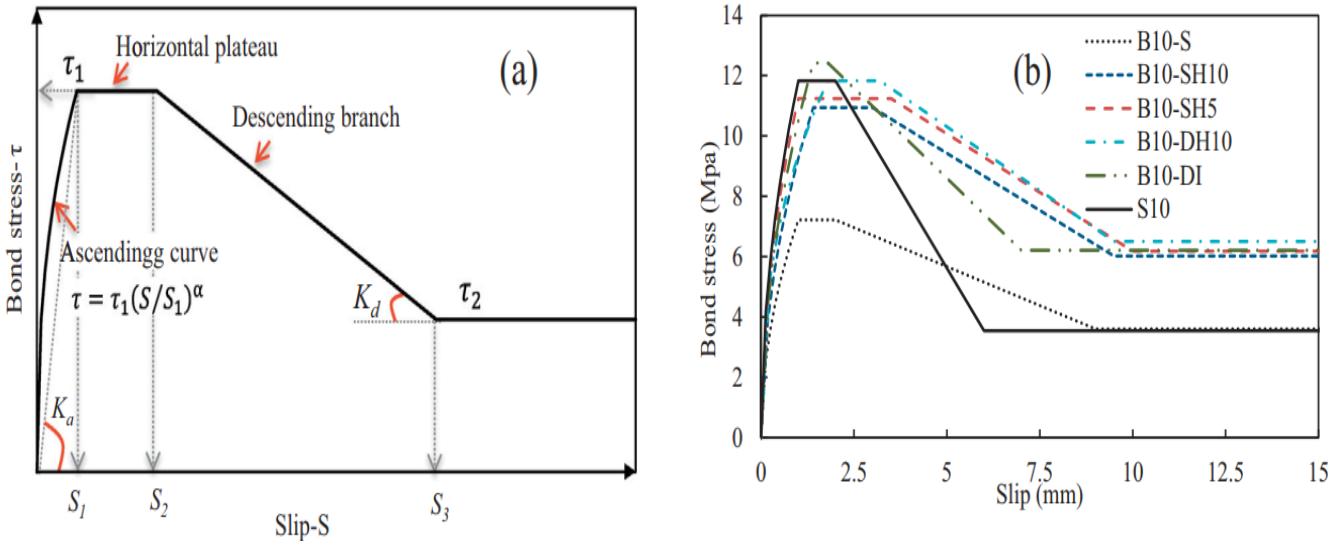

Fig. 7 (a) Bond–slip behavior of FRP bars[19], and (b) ribbed steel and BFRP bars bond–slip models under various surface conditions [20].

3.3 Loading and boundary conditions

In order to obtain a unique solution and guarantee that the finite element (FEA) model behaves similarly to the experimentally tested beam. Displacement boundary conditions must be applied at nodes in the center of the left support plates. While the displacement must be restricted in the Y and Z directions (Uy and Uz equal to zero). To optimize computing efficiency, just one quadrant of the beam was modeled, owing to the symmetry of the beam and the loading conditions. Consequently, symmetry boundary conditions were implemented on both planes of symmetry (the XZ plane and the YZ plane). All models were loaded at the identical locations as in the experimental test, using displacement-controlled load. The nonlinear analytical equations are solved using the "Newton-Raphson" equilibrium iteration technique, with a 0.05 displacement convergence criterion.

4. Test results and discussions

All beams reinforced with either basalt FRP or basalt fibers-steel wires composite bars exhibited comparable attitudes. However, the differences in the ratio of basalt fibers to steel wires led to variations in the crack's propagation, the ultimate load capacity, and the linear behavior, which is the most crucial characteristic of FRP beams. **Table. 4** detailed the experimental results and modes of failure of the tested beams.

Table. 4 Experimental results and failure mode of the tested beams.

Beam ID	RFT Type	Cracking Load P_{cr} (kN)	Cracking Deflection δ_{cr} (mm)	Ultimate Load P_u (kN)	Ultimate Deflection δ_u (mm)	Failure Mode
B1	S10	24.36	0.538	108.40	30.07	Concrete crushing after steel yielding
B2	B-SW-0	23.00	1.21	144.40	42.08	Concrete crushing while FRP rupture
B3	B-SW-20%	18.48	1.19	140.23	24.88	Concrete crushing
B4	B-SW-36%	20.73	1.014	152.10	22.85	Concrete crushing

4.1 Patterns of cracks and modes of failure

For all tested beams, the first crack propagated in the midspan of the tension side and developed vertically. However, as the applied load increased, two vertical cracks propagated and established gradually under the two concentrated loads at the outer boundaries of the maximum moment zone. As the load further increased, vertical and inclined cracks gradually extended upward. For beam B1, after the steel yielding load, cracks developed away from the flexural zone until the concrete strain reached its ultimate (ε_{cu}= 0.00305) and concrete crushing occurred. For the BFRP beam B2, the concrete also reached its ultimate strain (ε_{cu}= 0.003307) simultaneously with the BFRP bars rupturing and attaining their ultimate strain of 0.02527. Conversely, for both beams B3 and B4, the concrete reached its ultimate strain while the strains in the bottom bars for B3 and B4 were 0.0182 and 0.0171, respectively, which were still less than their maximum strains of 0.0216 and 0.0177, respectively. The experimental outcomes and failure modes are summarized in **Table 4.** Consequently, the FEA outlined the crack propagation and concrete crack patterns for tested beams at the failure load. At every integration point, a circle outlined with three perpendicular directions represented cracking and crushing in concrete elements. The red color represented the first crack, while the second and third cracks were colored with green and blue circle outlines, respectively. As shown in **Fig. 8**, there is a remarkable degree of agreement between the experimental and FEA crack patterns.

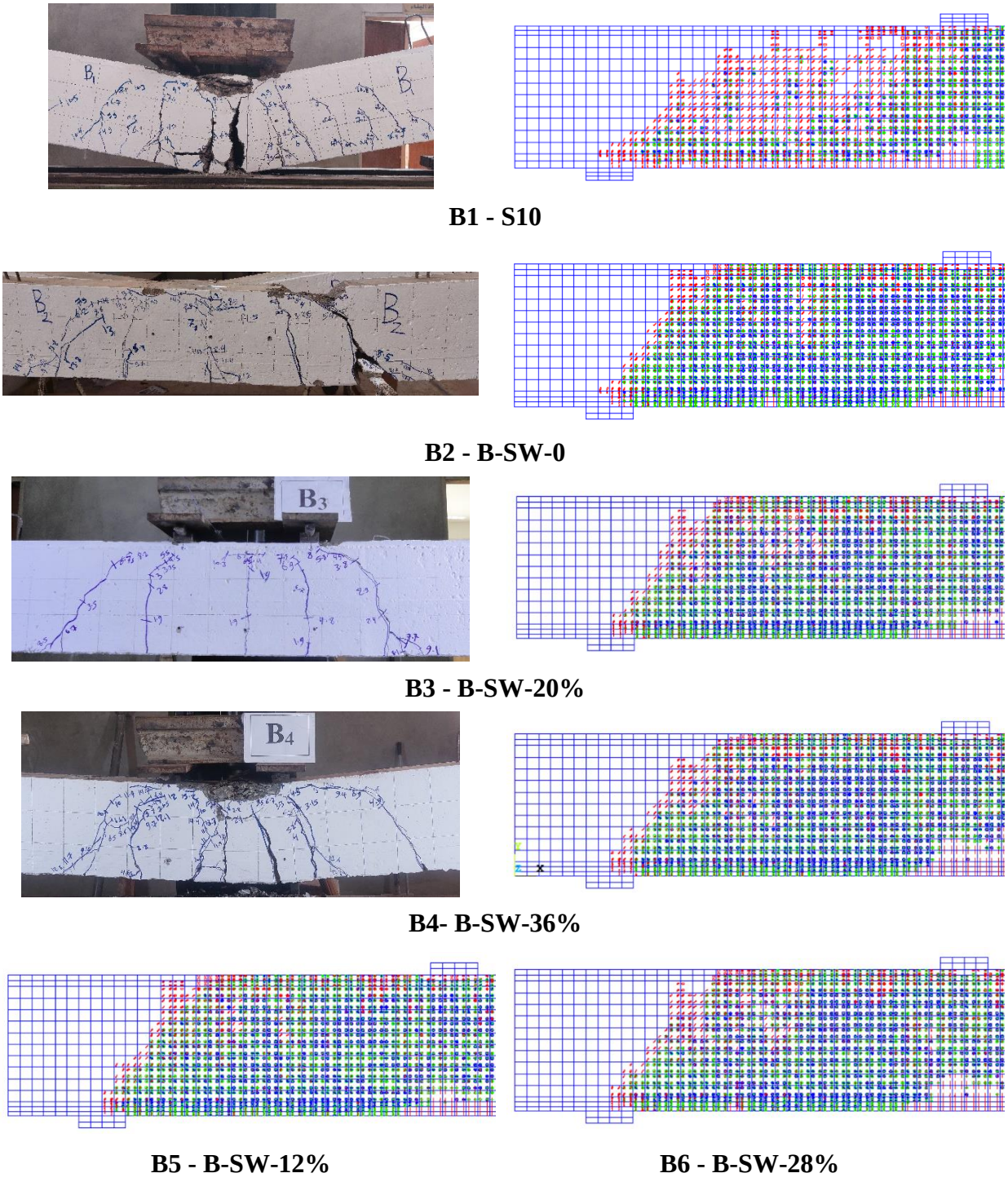

Fig. 8 Experimental and FEA crack patterns for the tested beams (B1, B2, B3, B4, B5 and B6).

4.2 Cracking and ultimate load capacity

Cracking loads for the beams B1, B2, B3, and B4 were determined to be 24.36, 23.00, 18.48, and 20.73 kN, respectively, where the cracking load mainly depended upon the concrete compressive strength, which was 37.8 MPa for B1 and B2 and 36.45 MPa for B3 and B4, as detailed in **Table. 4**. Furthermore, the ultimate load capacities for the reference beams B1 and B2 were 108.45 kN and 144.40 kN, respectively. Subsequently, employing B-SW-20% and B-SW-36% as the main

reinforcements for beams B3 and B4, respectively, had a marginal effect on their maximum load capacities. Specifically, for beam B3, the maximum load capacity was 140.23 kN, with a decreasing ratio of 3% compared to beam B2. This reduction in the maximum load capacity can be attributed to a decrease in the concrete compressive strength of B3 compared to B2, and its main reinforcement had a tensile strength of 1154.66 MPa less than 1242.16 for beam B2, as presented in **Table. 2**. Additionally, beam B4 recorded a maximum load capacity of 152.10 kN, a slight increase of 5% compared to B2.

Table. 5 organized the comparison of experimental and FEA results in terms of cracking and ultimate loads. For beams B1, B2, B3, and B4, the corresponding [Pcr_{EX} / Pcr_{FEA}] ratios were 0.98, 0.975, 0.793, and 0.89, respectively. Furthermore, as illustrated in **Fig. 9**, the ratios of [Pu_{EX} / Pu_{FEA}] for beams B1, B2, B3, and B4 were 1.04, 0.978, 1.003, and 0.972, respectively. Overall, the FEA model presented acceptable results, particularly in terms of the maximum load criteria, and it demonstrates that the ANSYS 15 [16] is a suitable tool for comprehending the behavior of reinforced concrete beams reinforced with either basalt FRP bars or basalt fiber-steel wire composite bars.

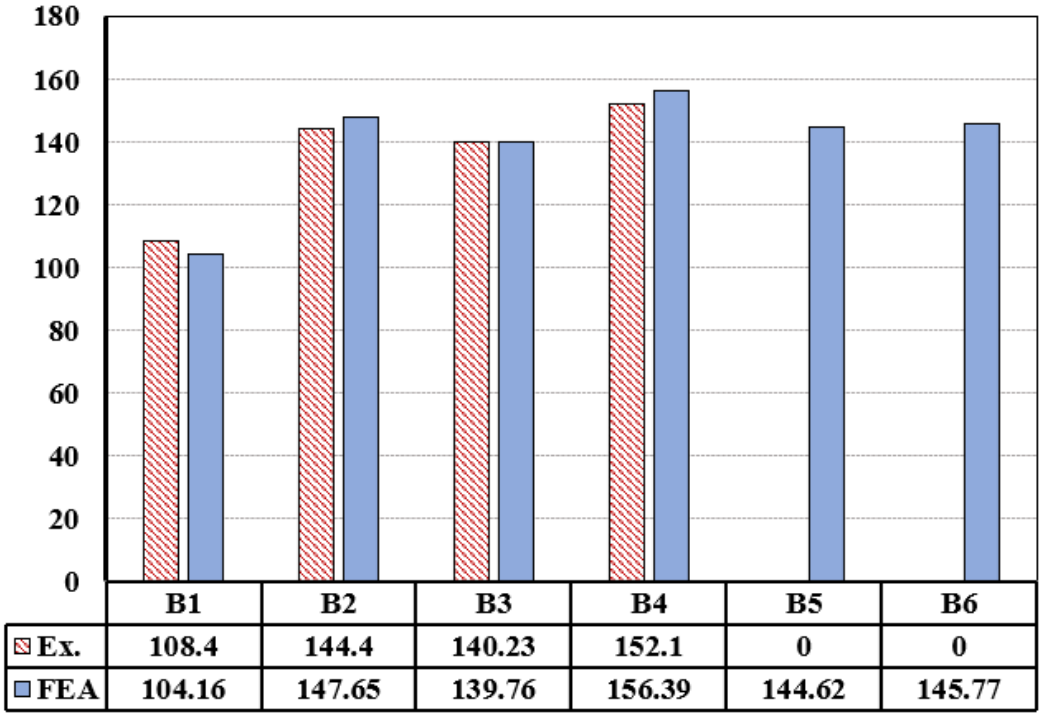

	B1	B2	B3	B4	B5	B6
Ex.	108.4	144.4	140.23	152.1	0	0
FEA	104.16	147.65	139.76	156.39	144.62	145.77

Fig. 9 Comparison between experimental and NLFEA in ultimate load results for tested beams.

4.3 Load-deflection behavior

The cracking and ultimate deflection values for tested beams are presented in **Table. 4**. In general, the tested beams exhibited similar behavior up to the point when initial cracks appeared. Beam B1 exhibited the lowest deflection at the cracking load; this can be attributed to the slip action between the concrete and steel reinforcement interface. Conversely, beam B2 exhibited the highest deflection at the cracking load. Further, the use of B-SW-20% and B-SW-36% within beams B3 and B4, respectively, resulted in a reduction in cracking deflection compared to beam B2. The ultimate deflections for beams B1 and B2 were 30.07 and 42.08 mm, respectively. However, a significant reduction in maximum deflection by 42% and 47% was observed when increasing basalt-fiber to steel wires ratio with 20% and 36% respectively. As shown in **Fig. 10**, the maximum

deflections for beams B3 and B4 were 24.88 mm and 22.85 mm respectively, due to the lower modulus of elasticity of their main reinforcement compared to beam B2. This reduction in the maximum deflection was accompanied by a notable decrease in cracks width, and considerable improvement in the beam's serviceability was noticed.

The Finite Element Analysis (FEA) model exhibited appropriate agreement with the experimental results. In particular, **Table. 5** shows that the ratios of experimental and FEA-predicted deflections for beams B1, B2, B3, and B4 were 1.07, 1.06, 0.84, and 0.916, respectively. Also, **Fig. 11**, **Fig. 12**, and **Fig. 13** graphically compare the load-deflection curves extracted from the FEA model and the experimental tests.

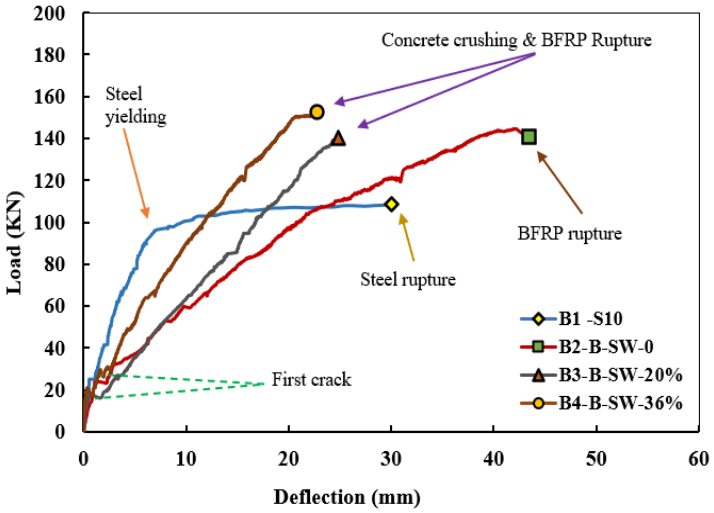

Fig. 10 Experimental load-deflection curve for tested beams.

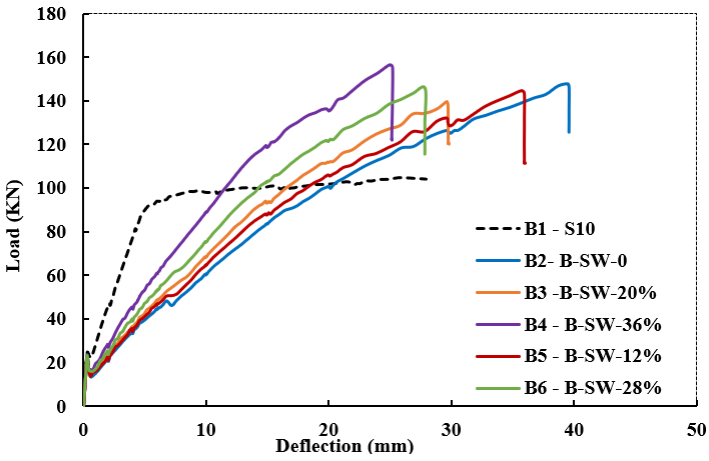

Fig. 11 FEA load deflection curve for tested beams.

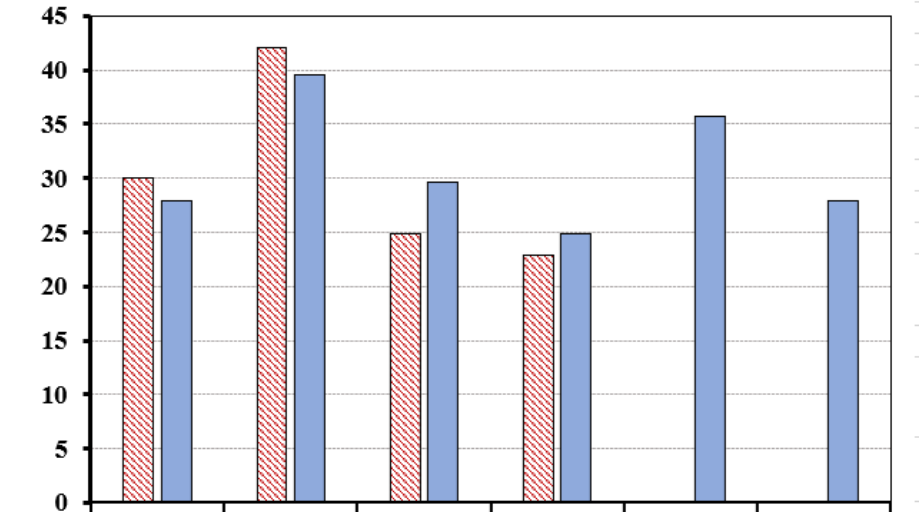

	B1	B2	B3	B4	B5	B6
Ex.	30.07	42.08	24.88	22.85	0	0
FEA	27.94	39.49	29.66	24.92	35.72	27.85

Fig. 12 Comparison between experimental and FEA in ultimate deflection results for tested beams.

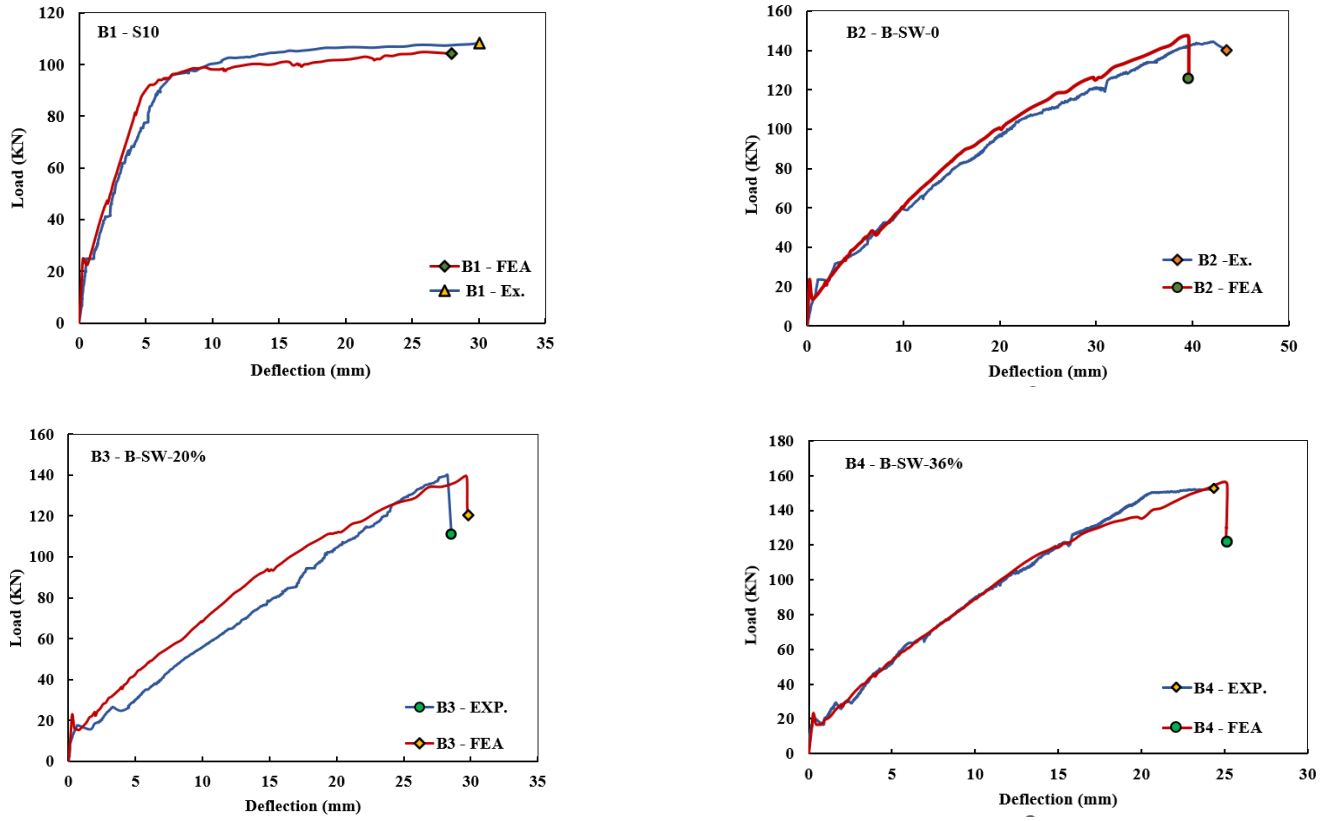

Fig. 13 Experimental and FEA mid span deflection for tested beams.

4.4 Strain in main reinforcement

The tensile strain response in the main reinforcement of tested beams was similar up to the cracking load and exhibited a linear behavior with a steep slope. Beyond this point, the high modulus of elasticity in steel kept the strain increment for B1 very small until it reached the yield point, at which point the strain rapidly increased. In contrast, the tensile strain for the beams B2, B3, and B4 was almost linear. **Fig. 14** depicts a sudden increase in tensile strain beyond the first crack, without a corresponding increase in the applied load. Where the reduction in the strain was decreased by further increasing the steel wires-to-basalt fibers ratio. This phenomenon is attributed to the transfer of tensile stress from the concrete to the main reinforcement following the concrete's cracking. Consequently, as shown in **Fig. 15**, the load-strain curves for beams B2, B3, and B4 demonstrated a linear behavior, where the total strain at failure decreased as the steel wire-to-basalt fiber ratio increased.

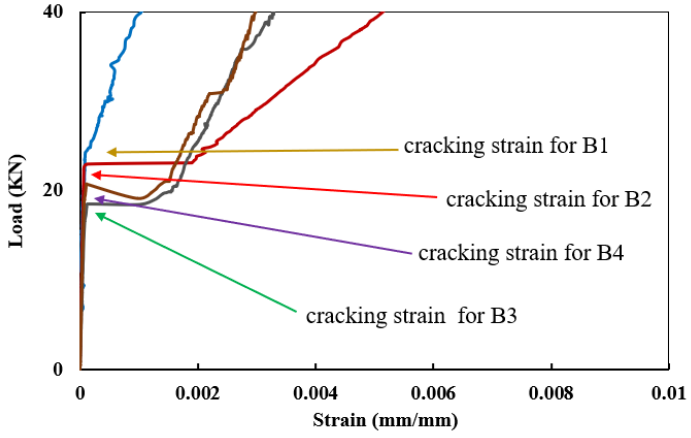

Fig. 14 Cracking strain for tested beams.

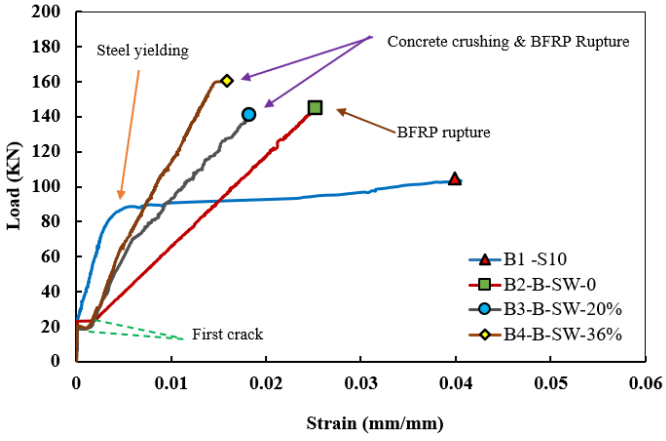

Fig. 15 Load – tensile strain for tested beams.

5. Theoretical analysis

Analytical methods were proposed to estimate the flexural capacity of tested beams according to ACI440.1R-15 [15] and ACI 318-19 [17]. All the beams reinforced with either basalt FRP bars or basalt fiber-steel wires composite bars were intended to be over-reinforced concrete sections, where the FRP reinforcement ratio (ρ_f) is exceeding 1.4 times the balanced ratio of the FRP reinforcement (ρ_{fb}) according to ACI440.1R-15 [15] as listed in **Table. 3**. While the beam B1 was under reinforced concrete section as (ρ_s) was less than (ρ_{max}) [17]. The balanced reinforcement ratios and the stress of tensile BFRP bars were estimated according to the following equations:

$$\boldsymbol{\rho_{fb}} = \mathbf{0.85}\boldsymbol{\beta_1}\frac{\boldsymbol{f_c^{\backslash}}}{\boldsymbol{f_{fu}}}\frac{\boldsymbol{E_f\varepsilon_{cu}}}{\boldsymbol{E_f\varepsilon_{cu}+f_{fu}}} \quad (1)$$

$$\boldsymbol{f_f} = \left(\sqrt{\frac{\left(\boldsymbol{E_f\varepsilon_{cu}}\right)^2}{\mathbf{4}}+\frac{\mathbf{0.85}\boldsymbol{\beta_1 f_c^{\backslash}}}{\boldsymbol{\rho_f}}\boldsymbol{E_f\varepsilon_{cu}}}-\mathbf{0.5}\boldsymbol{E_f\varepsilon_{cu}}\right)\leq \boldsymbol{f_{fu}} \quad (2)$$

$$M_n = A_f f_f\left(d-\frac{a}{2}\right)+A_s^{\backslash} f_y\left(d-d^{\backslash}\right) \quad (3)$$

Where A_f and f_f are the area and FRP bars tensile stress respectively. ρ_{fb} is the balanced reinforcement ratio, f_{fu} and E_f are the FRP ultimate tensile strength and modulus of elasticity respectively, $f_c^{\backslash}$ and ε_{cu} are the concrete compressive strength and ultimate strain respectively, and M_n is the nominal moment capacity for the tested beams. **Table. 5** clearly arranges the theoretical calculations for all tested beams.

Table. 5 Experimental, FEA and theoretical analysis.

Beam ID	First Cracking Load P_{cr} (KN)				Maximum Load P_u (KN)				Maximum Deflection (mm)		
	Ex.	FEA	Ex./FEA	Theo.	Ex.	FEA	EX./FEA	Theo.	Ex.	FEA	EX./FEA
B1	24.36	24.78	0.98	22.84	108.40	104.16	1.04	106.70	30.07	27.94	1.07
B2	23.00	23.59	0.975	22.84	144.40	147.65	0.978	138.48	42.08	39.49	1.06
B3	18.48	23.31	0.793	22.46	140.23	139.76	1.003	144.45	24.88	29.66	0.84
B4	20.73	23.46	0.89	22.46	152.10	156.39	0.972	161.90	22.85	24.92	0.916
B5	----	23.27	----	22.46	----	144.62	----	140.13	----	35.72	----
B6	----	23.36	----	22.46	----	145.77	----	150.48	----	27.85	----

6. Conclusions

This study presented an experimental investigation for the flexural performance of concrete members reinforced with locally manufactured basalt FRP bars and basalt fibers-steel wires composite bars. The findings derived from this experimental test were compared with numerical

analysis conducted with the ANSYS 15 [16], and theoretical analysis based on ACI440.1R-15 and ACI 318-19 guidelines. The following main conclusions can be arranged as follows:

1. Using basalt fibers-steel wires composite bars have a considerable effect on the deflection of the concrete beams. Where the deflection decreased by 42% and 47% by increasing basalt-fibers to steel wires ratio by 20% and 36% respectively. Therefore, a significant enhancement in the beam's serviceability were noticed.
2. The concrete members reinforced with either basalt FRP bars or basalt fibers-steel wires composite bars at first crack load exhibited a significant increase in both tension strains and deflection accompanied with a constant load level. However, the reinforcement strain and deflection decreased by increasing the steel wire ratio in composite bars.
3. Using basalt fibers-steel wires composite bars as main reinforcement have a slight effect on flexural load capacity. Where increasing the basalt fibers to steel wires ratio by 36% led to an increase in the beam's flexural load capacity by 5%.
4. The FEA model presented acceptable results and guarantees that the ANSYS 15 is a suitable way for comprehending the behavior of reinforced concrete beams reinforced with either basalt FRP bars or basalt fibers-steel wires composite bars.
5. The use of the design code provisions ACI440.1R-15 presented appropriate predictions for estimating the ultimate flexural capacity of concrete members reinforced with either basalt FRP or basalt fibers-steel wires composite bars.

Reference

[1] M. Alexander and H. Beushausen, “Durability, service life prediction, and modelling for reinforced concrete structures – review and critique,” Cem. Concr. Res., vol. 122, August, pp. 17–29, 2019, doi: 10.1016/j.cemconres.2019.04.018.

[2] F. Elgabbas, E. A. Ahmed, and B. Benmokrane, “Flexural Behavior of Concrete Beams Reinforced with Ribbed Basalt-FRP Bars under Static Loads,” J. Compos. Constr., vol. 21, no. 3, 2017, doi: 10.1061/(ASCE)CC.1943-5614.0000752.

[3] C. Li, H. Zhu, G. Niu, S. Cheng, Z. Gu, and L. Yang, “Flexural behavior and a new model for flexural design of concrete beams hybridly reinforced by continuous FRP bars and discrete steel fibers,” Structures, vol. 38, February, pp. 949–960, 2022, doi: 10.1016/j.istruc.2022.02.037.

[4] Y. H. Cui and J. Tao, “A new type of ductile composite reinforcing bar with high tensile elastic modulus for use in reinforced concrete structures,” Can. J. Civ. Eng., vol. 36, no. 4, pp. 672–675, 2009, doi: 10.1139/L09-012.

[5] X. Wang, Z. Wu, G. Wu, H. Zhu, and F. Zen, “Enhancement of basalt FRP by hybridization for long-span cable-stayed bridge,” Compos. Part B Eng., vol. 44, no. 1, pp. 184–192, 2013, doi: 10.1016/j.compositesb.2012.06.001.

[6] Y. Zeng, G. Wu, Z. Wu, and W. Feng, “Mechanical properties of steel wire-continuous basalt fiber composite plate (SBFCP) under monotonic tensile loading,” Appl. Mech. Mater., vol. 174–177, pp. 1471–1474, 2012, doi: 10.4028/www.scientific.net/AMM.174-177.1471.

[7] X. Wang, G. Wu, Z. Wu, Z. Dong, and Q. Xie, “Evaluation of prestressed basalt fiber and hybrid fiber reinforced polymer tendons under marine environment,” Mater. Des., vol. 64, pp. 721–728, 2014, doi: 10.1016/j.matdes.2014.07.064.

[8] D. W. Seo, K. T. Park, Y. J. You, and S. Y. Lee, “Experimental Investigation for Tensile Performance of GFRP-Steel Hybridized Rebar,” Adv. Mater. Sci. Eng., 2016, doi: 10.1155/2016/9401427.

[9] M. Fernand, I. Georges, and M. D. Zakari, “Effect of fiber volume ratio on flexural behavior

of RC beam with novel HFRP rebar and steel rebar," Structures, Vol 43, September, pp 1882-1900 , 2022, doi: 10.1016/j.istruc.2022.06.023.

[10] L. J. Guo, K. P. Zhou, X. C. Yang, G. S. Liu, and W. Y. Xu, "Experimental Study on the Mechanical Properties of FRP Bars by Hybridizing with Steel Wires," Adv. Mater. Res., vol. 941–944, no. June, pp. 2611–2619, 2014, doi: 10.4028/www.scientific.net/AMR.941-944.2611.

[11] M. Said, A. S. Shanour, T. S. Mustafa, A. H. Abdel-Kareem, and M. M. Khalil, "Experimental flexural performance of concrete beams reinforced with an innovative hybrid bars," Eng. Struct., vol. 226, February 2020, p. 111348, 2021, doi: 10.1016/j.engstruct.2020.111348.

[12] T. A. El-Sayed, A. M. Erfan, R. M. Abdelnaby, and M. K. Soliman, "Flexural behavior of HSC beams reinforced by hybrid GFRP bars with steel wires," Case Stud. Constr. Mater., vol. 16, p. e01054, 2022, doi: 10.1016/j.cscm.2022.e01054.

[13] Mohamed Abo Elyazed, R. Eltahawy, Omar A. EL-Nawawy., and K. S. Ragab, "Flexural Behavior of Concrete Slabs Reinforced with Innovative Semi-Ductile Hybrid FRP Bars," Int. J. Sci. Eng., vol. 10, no. 6, pp. 6–16, 2019.

[14] Y. M. Mohammad, A. E. A. Haridy, and A. El Thakeb, "Experimental Investigation on Mechanical Performance of Basalt Fiber-Steel Composite Bars," J. Al-Azhar Univ. Eng. Sect., vol. 19, no. 72, pp. 267–280, 2024, doi: 10.21608/auej.2024.258188.1561.

[15] ACI 440.1R, Guide for the Design and Construction of Structural Concrete Reinforced with Firber-Reinforced Polymer (FRP) Bars (ACI440.1R-15), vol. 22, no. 4. 2015. doi: 10.1016/0011-7471(75)90030-3.

[16] "ANSYS-Release Version 15.0, 'A Finite Element Computer Software and User Manual for Nonlinear Structural Analysis,' ANSYS Inc.," p. 15.

[17] I. Units, 318-19 Building Code Requirements for Structural Concrete and Commentary. 2019. doi: 10.14359/51716937.

[18] E. Hognestad, N. W. Hanson, and D. McHenry, "Concrete stress distribution in ultimate strength design," in Journal Proceedings, 1955, pp. 455–480.

[19] R. Eligehausen, E. P. Popov, and V. V Bertero, Local bond stress-slip relationships of deformed bars under generalized excitations. NTIS, 1983.

[20] A. M. A. IBRAHIM, M. F. M. FAHMY, and Z. WU, "Numerical Simulation on Fracturing Bond Mechanisms of Different Basalt FRP Bars," J. Japan Soc. Civ. Eng. Ser. A2 (Applied Mech., vol. 71, no. 2, p. I_289-I_298, 2015, doi: 10.2208/jscejam.71.i_289.